Electronic Structure of Selected {FeNO}^{7} Complexes in Heme and Non-Heme Architectures: A Density Functional and Multireference ab Initio Study

Mariusz Radoń,*,† Ewa Broclawik,‡ and Kristine Pierloot§

Faculty of Chemistry, Jagiellonian University, ul. Ingardena 3, 30-060 Kraków, Poland, Institute of Catalysis and Surface Chemistry, Polish Academy of Sciences, ul. Niezapominajek 8, 30-239 Kraków, Poland, and Department of Chemistry, University of Leuven, Celestijnenlaan 200F, B-3001 Heverlee-Leuven, Belgium

Received: October 26, 2009; Revised Manuscript Received: December 9, 2009

The multiconfigurational CASSCF/CASPT2 approach, along with various functionals of density functional theory, is applied to selected iron(II)−nitrosyl ({FeNO}^{7}) complexes, both with heme and nonheme groups. The energetics of the lowest doublet and quartet spin states at the correlated ab initio (CASPT2) level is presented for the first time. Comparison of the CASSCF and (unrestricted) DFT spin densities indicates that the nonhybrid functionals yield the spin densities most closely to the ab initio ones. The analysis of the multiconfigurational CASSCF wave function in terms of the localized active orbitals allows one to resolve the nature of Fe−NO bonding as a mixture of Fe(II)−NO^0 and Fe(III)−NO$^-$ resonance structures (in comparable contributions) for both spin states and various ligands.

1. Introduction

The electronic structure and properties of transition metal nitrosyl (NO) complexes are very much at the heart of bioinorganic chemistry. On one hand, nitric oxide is an intercellular signaling molecule, but on the other hand (at larger concentrations), it is also a poison.[1] For these reasons, there is great interest in the way NO interacts with the active centers of enzymes, particularly those containing Fe(II) (e.g., myoglobin, hemoglobin) or Fe(III) (e.g., the resting state of cytochrome P450). On the other hand, NO is an open shell and noninnocent ligand, providing transition metal nitrosyls with a complicated electronic structure, which is challenging both for experimental and computational studies.

In our previous theoretical study, we have investigated the binding energies of NO (together with CO and O_2) to model heme sites with Fe(II).[2] In the present paper, we focus more on the electronic structure and properties of the resulting iron(II)-nitrosyl complexes, denoted also as {FeNO}^{7} complexes after Enemark and Feltham.[3] (This notation reads that a total number of seven electrons, i.e., one free-radical electron from neutral NO and six electrons from the 3d orbitals of Fe(II), are distributed among the combinations of the NO π^* and Fe 3d orbitals and thus strongly delocalized on the FeNO fragment.) Theoretical electronic structure calculations on such complexes have received considerable interest recently.[2,4−8] Many of these studies, however, indicate that the widely used approximate density functional theory (DFT) methods often lead to inconclusive results with respect to the relative energies (and even the ordering) of low-lying states with different spins as well as to their spin density distributions.[2,4−6] These properties appear to be critically sensitive to the applied exchange-correlation functional, particularly to the exchange part. In addition, there are many controversies around the effective oxidation state of Fe and NO in {FeNO}^{7} groups. Depending on the spin state, coordination environment, and applied computational or experimental approach, various resonance structures have been postulated for {FeNO}^{7} complexes, including either Fe(II)−NO^0, Fe(III)−NO$^-$ (i.e., metal-to-ligand charge transfer), or even Fe(I)−NO$^+$ (i.e., ligand-to-metal charge transfer).[7,9−15]

The controversies around the {FeNO}^{7} systems motivated us to apply the multiconfigurational ab initio complete active space self consistent field/second-order perturbation theory (CASSCF/CASPT2) approach.[16,17] This multireference method has successfully been used to study several iron complexes, including systems of biological importance.[18−22] N.B., it yields NO binding energies to model heme Fe(II) complexes in reasonable agreement with experiment.[2] Herein, we apply the CASSCF/CASPT2 approach to several interesting complexes of the {FeNO}^{7} family, either with heme or nonheme groups. These are (**1**) FePNO, (**2**) FePImNO, (**3**) FePNH$_3$NO, (**4**) Fe(salen)NO, (**5**) Fe(5-Cl-salen)NO, (**6**) FeTNO$^-$, and (**7**) Fe(H$_2$O)$_5$NO^{2+} ("brown ring" complex), where P = porphyrin, Im = imidazole, salen = *N*,*N*′-ethylenebis(salicylimine), and T = tris(carbamoylmethyl)amine (see their structures in Figure 1). The heme nitrosyl complexes **1**−**3** are experimentally known to possess a doublet (S = 1/2) ground state.[14,23] Nevertheless, we also consider the excited quartet state (S = 3/2) for these complexes, as it seems very important for the kinetics of spin forbidden NO binding/dissociation[5,24] (the pathway involves an intersection between the ground doublet and the excited quartet state). Therefore, we believe that accurate calculation of the quartet−doublet splitting in these complexes is a prerequisite for future modeling of the NO binding pathway or dynamics. The quartet state is also crucial for the Fe(salen)NO complex (**4**), as this complex exhibits a thermal spin crossover from S = 1/2 to S = 3/2.[25] The nonheme complexes **6** and **7** are investigated only in their well established S = 3/2 ground state. The CASSCF wave functions for these model systems will be used to draw some conclusions about the electronic structure, spin densities, and effective oxidation states of Fe and NO, while the CASPT2 method (covering dynamic correlation) will be used to calculate the relative energies of the lowest doublet and quartet electronic states. An attempt will be made to compare CASSCF/CASPT2 results with standard DFT methods, and also

† Jagiellonian University.
‡ Polish Academy of Sciences.
§ University of Leuven.

10.1021/jp910220r
Published on Web 01/04/2010

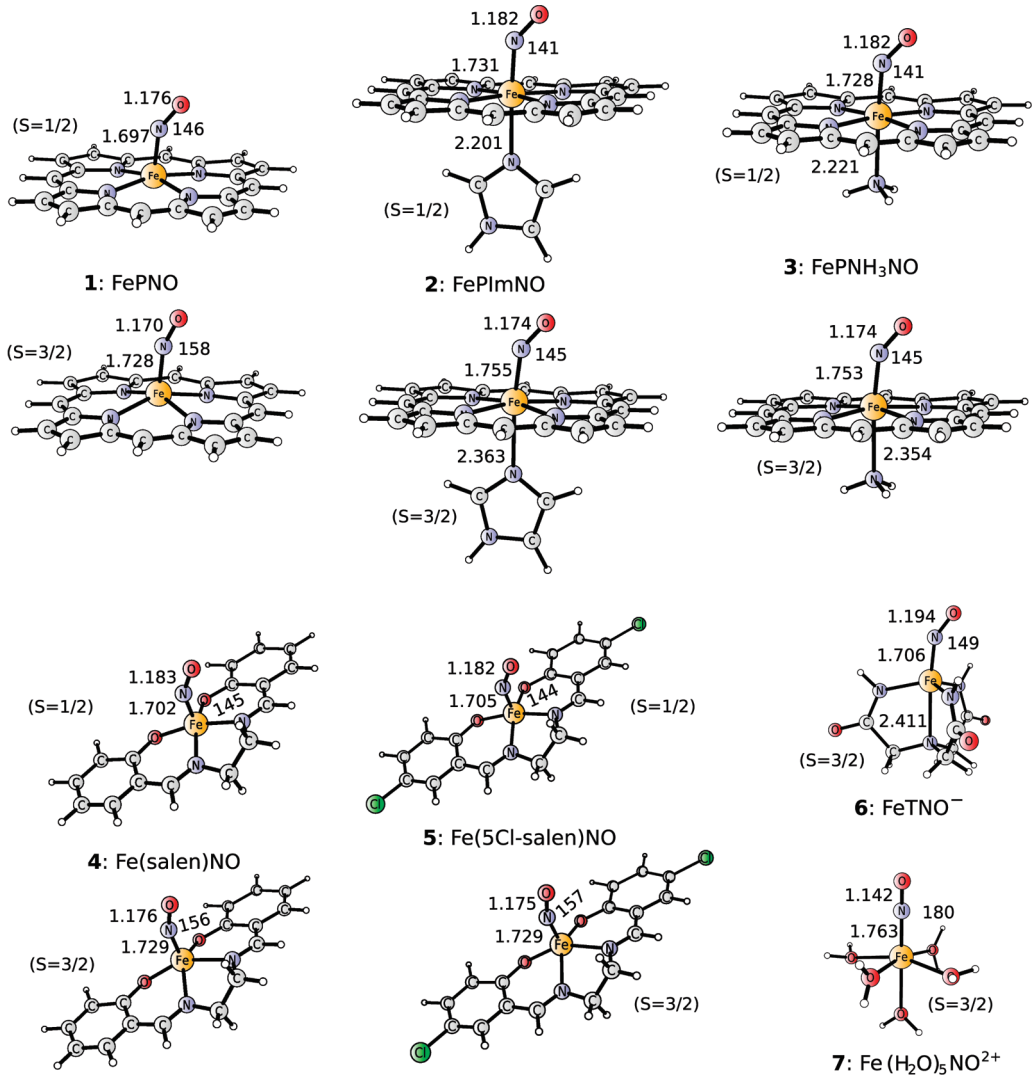

Figure 1. Structures of the model complexes from DFT:BP86/def2-TZVP optimization. The spin state is given within parentheses. Indicated values are Fe−N(O), N−O, and Fe−N(axial donor) distances (in angstroms) and Fe−N−O angle (in degrees).

with experimental data (wherever available), trying to draw some conclusions about the performance of various quantum chemical methods in this area.

2. Methods and Models

The structures of the complexes **1**−**7** are given in Figure 1. Structure optimizations at the DFT level were performed with either the Turbomole 5.9[26] or Gaussian 2003[27] package and employing def2-TZVP basis sets.[28] In view of the observed strong basis set dependence of DFT spin state energetics for some transition metal complexes,[20,29] we additionally performed single-point energy calculations with larger basis sets (composed of def2-QZVPP on Fe and def2-TZVPP on the ligands[28]). The latter energies are reported as "DFT results" below. The results agree to within ±1 kcal/mol with the smaller basis set results, thus indicating that the present DFT results can be considered converged with respect to the basis set. To cover the broad spectrum of popular DFT methods, several functionals were tested: from the widely used B3LYP functional containing 20% exact exchange,[30] through hybrids with a reduced contribution of exact exchange B3LYP*[31] (15%) and O3LYP[32] (10%), to the nonhybrid (GGA) functionals OLYP[33,34] and BP86.[35,36] All DFT calculations were performed as spin unrestricted. For both FePImNO and $FePNH_3NO$, unrealistic structures are obtained with the OLYP and O3LYP functionals, with the axial Im or NH_3 ligand either completely dissociated (both the $S = 1/2$ and $S = 3/2$ states of FePImNO and the $S = 3/2$ state of $FePNH_3NO$) or very loosely bound (the $S = 1/2$ state of $FePNH_3NO$, with an Fe−NH_3 distance of 3.75 Å). We further note that complexes similar to **2** are known experimentally.[14] Therefore, in our opinion, the structures of **2** and **3** arising from OLYP and O3LYP optimizations are unphysical. The OLYP and O3LYP results for these complexes reported below were therefore obtained from single-point calculations using the BP86 structures.

The optimized structures of **1**−**7** are given in Figure 1 (for the BP86 functional) and may also be found in the Supporting Information. All structures are oriented in such a way that the equatorial N or O atoms (of the P^{2-}, $salen^{2-}$, T^{4-}, or H_2O ligands) lie approximately in the *xy* plane, while the axial atoms (including the N atom of NO) are along the *z* axis. As confirmed by a vibrational analysis (BP86), most structures possess symmetric minima (at least C_s symmetry); in these cases, the *xz* plane was taken as the mirror plane. An exception is FePImNO in its $S = 3/2$ state, which revealed a small imaginary frequency and yielded a stable C_1 minimum with the Im ligand twisted by ∼40° and with an energy 0.14 kcal/mol lower than the C_s structure. However, as the difference in energy is immaterially small, we stuck to the symmetric structure as

TABLE 1: Contracted Basis Sets Employed in the CASSCF/CASPT2 Calculations

basis no.	Fe	"nearby" ligand atoms[a]	Cl	other heavy atoms	H
1[b]	7s6p5d2f1g	4s3p1d	4s3p2d	3s2p1d	2s
2[c]	7s6p5d3f2g1h	4s3p2d1f	5s4p2d	4s3p1d	3s1p
3[c]	10s9p8d6f4g2h	5s4p3d2f1g	5s4p3d1f	4s3p2d1f	3s2p1d

[a] The atoms of NO and of the first coordination sphere of Fe. [b] Basis 1 is derived from ANO-RCC[39] (Fe) and ANO-S[40] (ligands). [c] Bases 2 and 3 are derived from ANO-RCC.[39]

computationally simpler (particularly for CASPT2). A more important symmetry breaking was found for the Fe(salen)NO and Fe(5-Cl-salen)NO complexes: the nonsymmetric structures with a folded salen ligand have an energy lower by 3−4 kcal/mol than the C_s structures (used in a previous study[6]). This symmetry breaking is also clearly reflected by the crystal structure of Fe(salen)NO, where the salen ligand indeed has a folded ("stepped") conformation.[37] Therefore, in the present study, we employed the C_1 structures of complexes **4** and **5**. Unfortunately, except for the smallest basis set used in these calculations (see below), CASPT2 calculations for **4** and **5** were not feasible without symmetry. In order to estimate the CASPT2 results for the larger basis sets, we therefore obtained the CASPT2 distortion energy (upon $C_s \rightarrow C_1$ symmetry lowering) with the smallest basis sets, and used it to correct the energies of the symmetric structures obtained with the larger basis sets. This procedure should be accurate enough for the present purposes.

Single-point CASSCF/CASPT2 calculations were carried out for BP86 structures, making use of Molcas 7.[38] As ab initio calculations require very extensive basis sets to converge the dynamic correlation energy, we used three basis sets of increasing quality (basis 1−3) composed of atomic natural orbital (ANO) basis sets from the Molcas library[39,40] and shown in Table 1.

The active space used for the CASSCF/CASPT2 calculations follows the standard rules for transition metal compounds.[18,41] It is composed of Fe 3d (plus double-shell) and NO π^* orbitals, additionally supplemented with two extra ligand σ orbitals (i.e., those which mix with Fe $3d_{xy}$ and $3d_{z^2}$, therefore denoted as σ_{xy} and σ_{z^2}). The ligand orbitals must be active because of the partial covalent character of the metal−ligand bonds and associated non-dynamical (left−right) correlation.[18] Test calculations with alternative active spaces indicated that including the NO (bonding) π orbitals in the active space does not significantly influence the results of the present study. The resulting (11 in 14) active space was used for all calculations on the quartet states of complexes **1**−**5**, whereas for the doublet states of these complexes a smaller (11 in 13) space was used, obtained by removing a single double-shell orbital ($4d_{xy}$). The reason for doing so is that, with $3d_{xy}$ empty, $4d_{xy}$ would otherwise rotate into an empty ligand orbital (as we have checked previously, removal of the problematic $4d_{xy}$ orbital does not significantly influence the total energy of the low-spin state[2]). Both the $FeTNO^-$ complex **6** and the $Fe(H_2O)_5NO^{2+}$ complex **7** have significantly less covalent equatorial metal−ligand bonds than the other complexes, either because of the different character of the coordinating ligand atoms (oxygens in the case of complex **7**) or because of the trigonal symmetry of complex **6**, making the interaction of σ_{xy} with Fe 3d much weaker than that for complexes **1**−**5**. For complexes **6** and **7**, the σ_{xy} orbital is therefore no longer needed in the active space, and a smaller (9 in 13) space was used. More information about the active orbitals can be found in section 3.1 below and in the Supporting Information.

For a qualitative analysis of the wave functions, we used the results from basis 1 (CASSCF) or TZVP (DFT). Contour plots of the spin densities and Mulliken spin populations of the Fe and NO fragments were used to describe the spin density distributions obtained from CASSCF and DFT. We also performed a valence bond (VB)-like interpretation of the CASSCF wave function attempting to identify various resonance structures, such as $Fe(III)-NO^-$ or $Fe(II)-NO^0$, contributing to the CAS wave function. Hereto, each participating configuration state function (CSF) was classified in terms of its resonance structure by counting the number of electrons in the orbitals of predominant Fe or NO character. Next, the *total* weight of all CSFs contributing to a given resonance structure was calculated. In a similar way, the antiferromagnetic character of the CAS wave function was determined, by calculating the total weight of the CSFs with a local spin on Fe larger than the total spin, the difference being compensated by antiferromagnetic coupling with unpaired electron(s) on NO. Only CSFs with a coefficient larger than 0.04 were included in these analyses (this suffices to reproduce about 90% of the CAS wave function). The analyses cannot, however, be performed for the CI expansion in terms of the CASSCF natural orbitals, as the latter are strongly delocalized (due to strong covalent interactions between NO π^* and Fe 3d), and thus cannot be classified as either Fe-like or NO-like. Therefore, we instead used the CAS CI expansion in terms of localized orbitals, obtained (using the Cholesky algorithm[42]) as proper combinations of the CASSCF natural orbitals. Only the natural orbitals with a significant NO π^* contribution were included in the localization (for most cases, the five natural orbitals being the combinations of Fe $3d_{xz,yz,z^2}$ and NO $\pi^*_{x,y}$; more information can be found in the Supporting Information). The orbitals resulting from the localization turned out to be almost pure Fe 3d or NO π^* (see the contour plots of the localized orbitals given in the Supporting Information). Note that the transformation to such a set of localized orbitals (obtained as combinations of the active orbitals) does not change the overall CAS wave function but only simplifies its intuitive interpretation in terms of VB-like contributions.

The adiabatic relative quartet (Q)−doublet (D) energy was calculated for complexes **1**−**5** directly from the electronic energies of the respective states at their optimized structures. This property will be denoted as the *electronic quartet−doublet gap* (ΔE_{el}). However, the relative stability of these states is rather determined by the quartet−doublet Helmholtz free energy

$$\Delta F = F_Q - F_D = \Delta E_{el} + \Delta F_{therm} \qquad (1)$$

which, in addition to ΔE_{el}, contains a thermodynamical correction, ΔF_{therm}, accounting for the difference in vibrational frequencies between the doublet and quartet electronic states. In brief, some metal−ligand bonds have a smaller force constant in the quartet than the doublet state (because the antibonding Fe d_{xy} orbital becomes occupied in the quartet state, see section 3.1). Consequently, the frequency of the associated vibration(s)

TABLE 2: Thermodynamical Correction (ΔF_{therm}) to the Quartet−Doublet Relative Free Energy (in kcal/mol) Calculated for Several Temperatures

T (K)	FePNO (**1**)	FePImNO (**2**)	$FePNH_3NO$ (**3**)	Fe(salen)NO (**4**)	Fe(5-Cl-salen)NO (**5**)
0	–1.7	–1.9	–2.0	–1.5	–1.5
175.0	–2.4	–2.6	–2.4	–2.2	–2.4
298.15	–3.3	–3.4	–3.0	–3.0	–3.3

is also lower, thus giving the quartet a higher vibrational entropy and a lower vibrational energy than the doublet state. In general, $\Delta F_{therm} < 0$ and $|\Delta F_{therm}|$ is an increasing function of temperature. Although ΔF_{therm} is sometimes neglected, we believe it is important for quantitative considerations. An important point is that the temperature dependence of the ΔF_{therm} term is the driving force for the thermal spin crossover phenomenon (ΔE_{el} is temperature independent).[43,44] At the spin crossover temperature (T_c), $\Delta F = 0$ in eq 1; thus, one can obtain the condition:

$$\Delta E_{el} = -\Delta F_{therm}(T_c) \tag{2}$$

which will be used to provide an "experimental" estimation of the electronic quartet−doublet gap based on the experimental crossover temperature (T_c). As ΔF_{therm} in eq 2 relies on the theoretical (DFT) calculation of vibrational frequencies, this approach is, strictly speaking, not fully experimental. However, ΔF_{therm} is much less sensitive to the computational approach (choice of the functional) than the ΔE_{el} term (see section 3.3). In fact, any DFT calculation provides a good approximation for $\Delta F_{therm}(T_c)$, at least up to chemical accuracy. Keeping this in mind, we shall refer to the quartet−doublet gaps obtained with the aid of eq 2 as to "experimental results".

The ΔF_{therm} values calculated for several temperatures are given in Table 2. The calculations employed the (unscaled) BP86 frequencies and standard expressions from statistical mechanics as implemented in Turbomole.[26] The (very small) contribution to the relative entropy caused by the different degeneracies of $S = 1/2$ and $S = 3/2$ electronic states was also included. For the $S = 3/2$ state of FePImNO, we used the frequencies of the nonsymmetric structure (as explained above, the symmetric structure has an imaginary frequency).

3. Results and Discussion

3.1. Electronic Structure at the CASSCF Level. Let us first focus on the electronic structure of the studied {FeNO}^{7} complexes. To this end, we must take a closer look at the active orbitals and principal CASSCF configurations, given schematically in Figure 2 for the example of FePNO. Qualitatively, the same picture holds for all complexes, with some differences indicated in the discussion below. Contour plots of the active orbitals for all complexes can be found in the Supporting Information.

One of the Fe d orbitals, $d_{x^2-y^2}$, essentially does not interact with the ligand orbitals. Another one, d_{xy}, is strongly destabilized by the equatorial ligand field. In a similar way, the d_{z^2} orbital is destabilized by the axial ligand field. Due to its trigonal symmetry, the situation of complex **6** is slightly different: both the $d_{x^2-y^2}$ and d_{xy} orbitals are destabilized by the ligand field, though much less than for the other complexes (nonoptimum overlap with the ligand orbitals). A key issue for the electronic structure of the {FeNO}^{7} group is the quite strong covalent interaction between three Fe d orbitals (d_{xz}, d_{yz}, and d_{z^2}) and both NO $\pi^*_{x,y}$ orbitals. It leads to two bonding orbitals $(d,\pi^*_{x,y})_b$, two antibonding orbitals $(d,\pi^*_{x,y})_a$, and one nonbonding orbital $(d,\pi^*_x)_n$. This qualitative picture holds for all complexes, except for complex **7**: with a linear NO coordination, the interaction between Fe d_{z^2} and NO π^* becomes symmetry-forbidden, and the nonbonding $(d,\pi^*_x)_n$ orbital therefore becomes pure Fe d_{z^2}. [Let us note that also for the other complexes in the $S = 3/2$ state the nonbonding $(d,\pi^*_x)_n$ orbital appears to be dominated by d_{z^2}, the nonzero contribution of π^* being significantly smaller than in the corresponding $(d,\pi^*_x)_n$ orbital for the $S = 1/2$ state.] However, for the sake of simplicity, we shall consequently use the "$(d,\pi^*_x)_n$" notation for all complexes.

Using the CASSCF natural orbitals, the principal configurations for the doublet ($S = 1/2$) and quartet ($S = 3/2$) electronic states can be written as

$$^2\Phi_0 = |(d_{x^2-y^2})^2(d_{xy})^0(d,\pi^*_x)^1_n(d,\pi^*_x)^2_b(d,\pi^*_y)^2_b(d,\pi^*_x)^0_a(d,\pi^*_y)^0_a\rangle \tag{3}$$

$$^4\Phi_0 = |(d_{x^2-y^2})^1(d_{xy})^1(d,\pi^*_x)^1_n(d,\pi^*_x)^2_b(d,\pi^*_y)^2_b(d,\pi^*_x)^0_a(d,\pi^*_y)^0_a\rangle \tag{4}$$

as also depicted in Figure 2. Note that the doublet-to-quartet transition merely corresponds to the excitation of an electron from $d_{x^2-y^2}$ to d_{xy} on iron. Therefore, the quartet−doublet gap (more of which in section 3.3) must to a large extent depend on the strength of the equatorial ligand field, as manifested by the energy separation between the d_{xy} and $d_{x^2-y^2}$ orbitals.

The weights of the principal $^{2,4}\Phi_0$ configurations in the CAS wave function are significantly below 100%: 76−78.5% for $S = 1/2$ and 60−61% for $S = 3/2$. The remaining 20−40% of the wave function is distributed over many configurations, none of which reaches a contribution larger than 10%. Among the most important configurations are the double excitations from the $(d,\pi^*)_b$ to $(d,\pi^*)_a$ orbitals, pointing to a strong left−right correlation in the Fe−NO bond. The latter is also reflected by the occupation numbers of the bonding and antibonding $(d,\pi^*)_{b,a}$ orbitals, being very different from the formal values 2 (bonding) and 0 (antibonding), i.e., 1.8 (bonding) and 0.2 (antibonding)

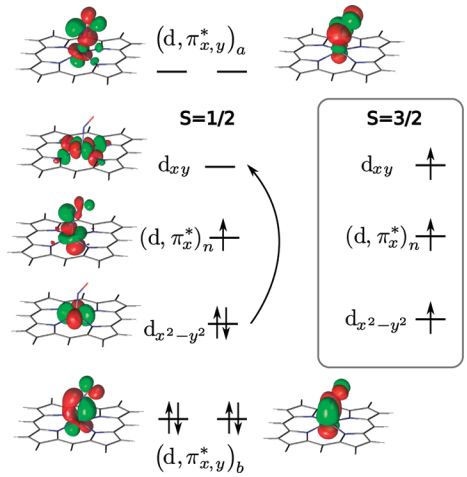

Figure 2. CASSCF natural orbitals and principal electronic configurations on the example of FePNO.

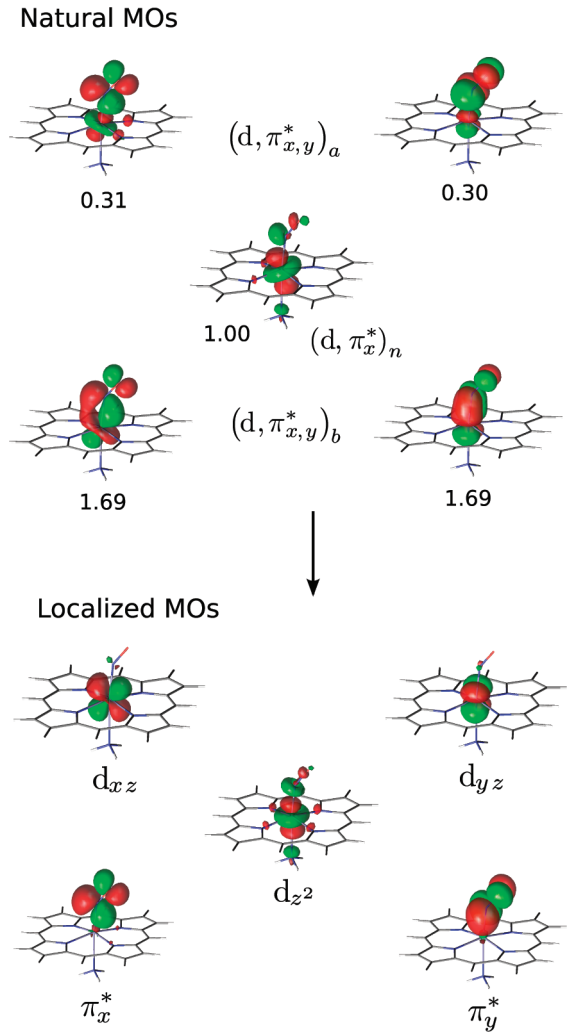

Figure 3. Selected Fe−NO orbitals, before and after Cholesky localization, for the example of (S = 3/2) $FePNH_3NO$.

for S = 1/2 and 1.7 (bonding) and 0.3 (antibonding) for S = 3/2. Interestingly, for each of the two $(d,\pi^*)_{b,a}$ pairs, the sum of the occupation numbers for the bonding and the antibonding orbital is very close to two electrons.

As we shall see in section 3.2, all complexes have a strongly polarized spin density in their quartet state, with excess spin-up density on Fe and excess spin-down density on NO (cf. Figure 5). However, the dominant configuration $^4\Phi_0$ given above (eq 4) has only three unpaired electrons on Fe; therefore, it cannot explain the observed spin polarization. The polarization emerges from an admixture of formally excited $(d,\pi^*)_b \rightarrow (d,\pi^*)_a$ configurations. Mixing of these configurations with the principal configuration $^4\Phi_0$ induces antiferromagnetic character in the total CAS wave function. The antiferromagnetic character becomes clear after performing an orbital localization procedure (see section 2 for details), leading to separation of the strongly interacting Fe 3d and NO π^* orbitals (for different complexes, a similar procedure was used in ref 21). Figure 3 shows both the natural (delocalized) and the localized orbitals for the case of $FePNH_3NO$ (S = 3/2); similar figures for the other complexes may be found in the Supporting Information. In terms of localized orbitals, the CAS wave function becomes a combination of three important contributions:

$$^4\Phi'_1 = |(d_{x^2-y^2})^{\uparrow}(d_{xy})^{\uparrow}(d_{z^2})^{\uparrow}(d_{xz})^{\uparrow}(d_{yz})^{\uparrow}(\pi^*_x)^{\downarrow}(\pi^*_y)^{\downarrow}\rangle \quad (5a)$$

$$^4\Phi'_2 = |(d_{x^2-y^2})^{\uparrow}(d_{xy})(d_{z^2})^{\uparrow}(d_{xz})^{\uparrow}(d_{yz})^2(\pi^*_x)^{\downarrow}(\pi^*_y)^0\rangle \quad (5b)$$

$$^4\Phi'_3 = |(d_{x^2-y^2})^{\uparrow}(d_{xy})^{\uparrow}(d_{z^2})^{\uparrow}(d_{xz})^2(d_{yz})^{\uparrow}(\pi^*_x)^0(\pi^*_y)^{\downarrow}\rangle \quad (5c)$$

each of them, indeed, pointing to antiferromagnetic coupling between Fe (spin-up) and NO (spin-down).[45] Configuration $^4\Phi'_1$ has Fe(III) (S_{Fe} = 5/2)−NO^- (S_{NO} = 1) character; the other two configurations have Fe(II) (S_{Fe} = 2)−NO^0 (S_{NO} = 1/2) character. For complexes **1**−**6**, the $^4\Phi'_1$ configuration contributes about 40−45% to the CAS wave function and $^4\Phi'_2$ and $^4\Phi'_3$ together about 30−40%. The exception is the "brown ring" complex (**7**), which has more $^4\Phi'_2$ and $^4\Phi'_3$ (together about 60%) and less $^4\Phi'_1$ (only 20%) character.

To get further insight into the CAS wave function, we repeated the orbital localization procedure also for the doublet state of complexes **1**, **3**, and **4**. Unfortunately, this resulted in rather long (diffuse) CAS CI expansions. Among the main contributions, there are some of Fe(III)−NO^- character, e.g.,

$$^2\Phi'_1 = |(d_{x^2-y^2})^2(d_{xy})^0(d_{z^2})^{\uparrow}(d_{xz})^{\uparrow}(d_{yz})^{\uparrow}(\pi^*_x)^{\downarrow}(\pi^*_y)^{\downarrow}\rangle \quad (6a)$$

$$^2\Phi'_2 = |(d_{x^2-y^2})^2(d_{xy})^0(d_{z^2})^0(d_{xz})^2(d_{yz})^{\uparrow}(\pi^*_x)^{\uparrow}(\pi^*_y)^{\downarrow}\rangle \quad (6b)$$

as well as some of Fe(II)−NO^0 character, e.g.,

$$^2\Phi'_3 = |(d_{x^2-y^2})^2(d_{xy})^0(d_{z^2})^{\uparrow}(d_{xz})^2(d_{yz})^{\uparrow}(\pi^*_x)^0(\pi^*_y)^{\downarrow}\rangle \quad (7a)$$

$$^2\Phi'_4 = |(d_{x^2-y^2})^2(d_{xy})^0(d_{z^2})^{\uparrow}(d_{xz})^{\uparrow}(d_{yz})^2(\pi^*_x)^{\downarrow}(\pi^*_y)^0\rangle \quad (7b)$$

$$^2\Phi'_5 = |(d_{x^2-y^2})^2(d_{xy})^0(d_{z^2})^0(d_{xz})^2(d_{yz})^2(\pi^*_x)^{\uparrow}(\pi^*_y)^0\rangle \quad (7c)$$

$$^2\Phi'_6 = |(d_{x^2-y^2})^2(d_{xy})^0(d_{z^2})^{\uparrow}(d_{xz})^2(d_{yz})^{\downarrow}(\pi^*_x)^0(\pi^*_y)^{\uparrow}\rangle \quad (7d)$$

As previously, some configurations ($^2\Phi'_1$, $^2\Phi'_3$, and $^2\Phi'_4$) describe antiferromagnetic coupling either between Fe(III) (S_{Fe} = 3/2) and NO^- (S_{NO} = 1) or between Fe(II) (S_{Fe} = 1) and NO^0 (S_{NO} = 1/2), but let us also note the presence of configurations like $^2\Phi'_5$ and $^2\Phi'_6$, describing a singlet Fe(II) and an unpaired electron on NO^0. The weights of various configurations in the basis of localized orbitals are given in the Supporting Information.

To deal with a large number of configurations, we calculated the *collective* weights of all configurations belonging to a given resonance structure (like Fe(II)−NO^0), thereby obtaining weights of participating resonance structures. Decomposition of the CASSCF wave function in terms of the resonance structures is given as a histogram plot in Figure 4. (Please note that the results for FePImNO and Fe(5-Cl-salen)NO are almost the same as those for $FePNH_3NO$ and Fe(salen)NO, respectively; therefore, they are not presented in Figure 4.) As is evident from Figure 4, all complexes are best characterized as mixtures of Fe(II)−NO^0 and Fe(III)−NO^- resonance structures. For complexes **1**−**6**, these two structures have a comparable contribution, and only the "brown ring" complex (**7**) has more pronounced Fe(II)−NO^0 character (in agreement with some previous

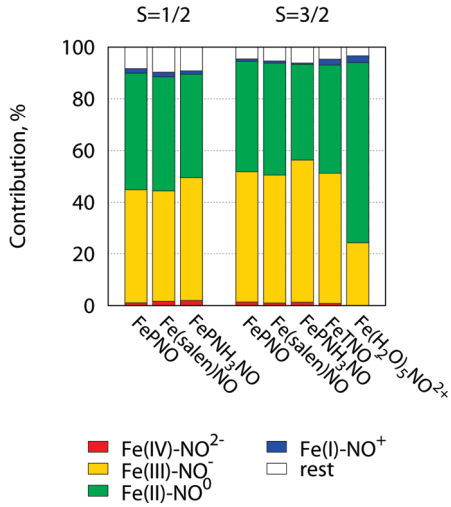

Figure 4. Analysis of the CAS wave functions in terms of Fe−NO resonance structures.

claims[7]). We note that the present assignment of Fe in the studied {FeNO}^{7} groups as a mixture of Fe(II) and Fe(III) agrees with Mössbauer spectra of the {FeNO}^{7} $S = 3/2$ groups in several similar complexes, yielding an isomer shift of Fe between the values characteristic for Fe(II) and Fe(III).[12] We therefore cannot agree with some claims in the literature[6,11,46] that the quartet state of the {FeNO}^{7} complexes is predominantly Fe(III)−NO$^-$. Clearly, for all complexes studied here, this resonance structure is important, but the contribution of Fe(II)−NO^0 is of comparable importance. Moreover, the contribution of Fe(II)−NO^0 and Fe(III)−NO$^-$ is almost the same for both spin states (complexes **1**−**5**). This is in agreement with our previous remark about the nature of the 1/2 → 3/2 transition in the {FeNO}^{7} complexes, which is predominantly an internal promotion on Fe ($d_{x^2-y^2}$ → d_{xy}, cf. Figure 2). Naturally, such internal excitation on Fe should not affect significantly the oxidation states of the Fe and NO fragments. This observation also conforms to the very similar N−O distances obtained for the $S = 1/2$ and $S = 3/2$ states of complexes **1**−**5** (cf. Figure 1): If the quartet state had significantly more Fe(III)−NO$^-$ character than the doublet state, its N−O distance would have to be longer (due to an increased population of the antibonding NO π^* orbitals).[15] In fact, the N−O distance is almost the same in both spin states (even slightly shorter in the quartet).

Figure 4 further indicates that besides Fe(II)−NO^0 and Fe(III)−NO$^-$ the other, more exotic, resonance structures are of marginal importance for the complexes studied. We have found only a few % of the previously suggested Fe(I)−NO$^+$ structure.[2,9,10,13,14] In other words, the "Fe(I)−NO$^+$" description should merely be regarded as a formal one. In reality, the extremely strong d → π^* back-donation repopulates the "empty" NO π^* orbitals and changes the real oxidation number of Fe to between II and III.

It was already mentioned that the antiferromagnetic (Fe−NO) configurations have an important contribution to the CAS wave function. To quantify this effect, we have summed the total contribution of these configurations for complexes **1**, **3**, and **4**, thus obtaining a measure of antiferromagnetic character in the CAS wave function (Table 3). A first glimpse at Table 3 already shows that the antiferromagnetic character is more pronounced for the quartet than for the doublet electronic state. Among the $S = 1/2$ complexes, the six-coordinate complex (**3**) has the smallest contribution of antiferromagnetic configurations. These observations will be useful for the interpretation of the DFT spin densities in the next section.

TABLE 3: Antiferromagnetic Fe−NO Character (%) of the CAS Wave Functions

	FePNO (**1**)	$FePNH_3NO$ (**3**)	Fe(salen)NO (**4**)
($S = 1/2$)	58.9	38.9	60.8
($S = 3/2$)	82.6	80.9	83.6

3.2. Spin Densities. It was already pointed out previously that DFT spin densities of {FeNO}^{7} can be extremely sensitive to the choice of the functional.[2,5,6] In order to resolve the ambiguous DFT results, we have calculated spin densities at the CASSCF level, given in Figure 5. The analysis is limited to three representative complexes: (**1**) FePNO (five-coordinate heme), (**3**) $FePNH_3NO$ (six-coordinate heme), and (**4**) Fe(salen)NO (five-coordinate nonheme). The spin densities of FePImNO and Fe(5-Cl-salen)NO are very similar to those of $FePNH_3NO$ and Fe(salen)NO, respectively, and will therefore not be discussed separately. Also, the spin densities of $S = 3/2$ $FeTNO^-$ and $Fe(H_2O)_5NO^{2+}$ are analogous to the other complexes in their quartet state. CASSCF spin populations of Fe and NO for all complexes can be found in the Supporting Information.

According to CASSCF (Figure 5), the $S = 1/2$ state of the five-coordinate systems has an Fe spin population close to 1.0, while the NO fragment does not carry any significant spin density. This picture holds both for FePNO and Fe(salen)NO, irrespective of the different coordination environment of iron in these complexes (i.e., four nitrogens versus two nitrogens and two oxygens). In contrast, and in agreement with previous observations,[2,5,47] coordination of the axial N donor in complex **3** shifts about 30% of the spin density toward NO (mostly to the π_x^* orbital). The large, positive spin density on NO for **3** can be partially explained by a relatively large contribution of the $^2\Phi_5'$ configuration (eq 7d in section 3.1), describing a closed shell Fe(II) and a NO radical.

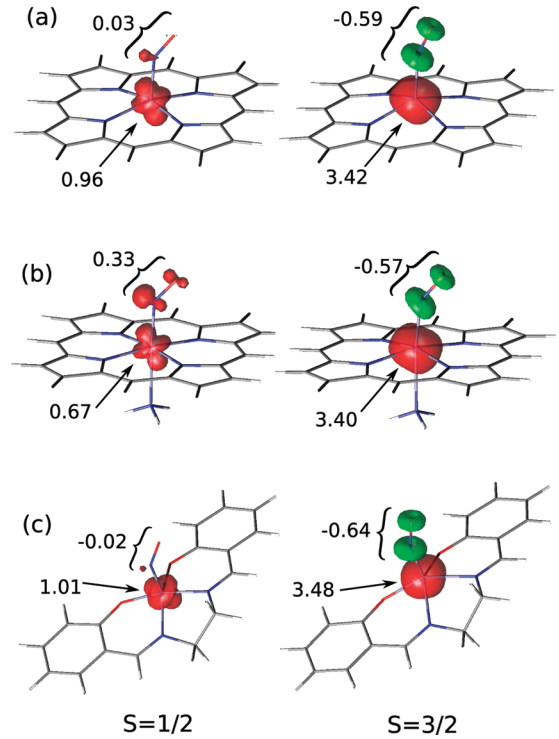

Figure 5. CASSCF spin densities for the doublet (left) and quartet state (right) of (a) FePNO, (b) $FePNH_3NO$, and (c) Fe(salen)NO, given as contour plots (for 0.02 b^{-3} isovalue) and Mulliken spin population on Fe and NO.

The CASSCF spin densities of **1** and **3** are in excellent agreement with the interpretation of magnetic circular dichroism (MCD)[14,23] and electron paramagnetic resonance (EPR)[48] experiments. First, the MCD spectrum of the five-coordinate heme−NO complex is dominated by a **C**-term contribution, indicating a large influence of spin orbit coupling, which reads that the spin density is predominantly localized on the heavy (iron) atom.[14,23] In contrast, all three (**A**, **B**, and **C**) terms of the MCD spectrum become important for six-coordinate heme, indicating a shift of spin density toward the NO ligand,[14,23] as also observed in our CASSCF calculations. Second, from the EPR spectrum of the five-coordinate heme−NO complex, more specifically from the isotropic ^{14}N hyperfine coupling constant, only 10% of the spin density appears to be localized on NO, while the rest must reside in FeP.[48] Moreover, the lowest g_{zz} value is very close to the free electron value. According to a qualitative model from McGarvey,[49] this means that the unpaired electron is localized mostly in the d_{z^2} orbital of Fe.[48] This is in close agreement with the CASSCF spin density and the principal configuration $^2\Phi_0$ in the CAS CI expansion for FePNO (eq 3 in section 3.1).

As opposed to the variety of spin densities observed for the doublet state, all complexes have very similar spin densities in their lowest quartet state. These densities exhibit characteristic spin polarization with (majority) spin-up density on Fe and (minority) spin-down density on NO, a pattern which is not modified by coordination of the axial ligand (see Figure 5). A more careful look would reveal that the minority spin density of NO is distributed in both $\pi^*_{x,y}$ orbitals, thus yielding the characteristic cylindrical contour around NO. As already pointed out, the spin polarization stems from the strong antiferromagnetic character of the $S = 3/2$ wave function (about 80%), more pronounced than for the doublet state (cf. Table 3 in section 3.1). Comparing the message of Table 3 with Figure 5, it might seem surprising that for the doublet state the antiferromagnetic character (∼40−60%) does not lead to a spin polarization, similar to the one for the quartet state; instead of the expected negative (spin-down) spin density, NO bares almost no spin density (complexes **1** and **4**) or even positive (spin-up) spin density (complex **3**). This apparent ambiguity can be clarified if one notes that although the three most important doublet configurations ($^2\Phi'_1$, $^2\Phi'_3$, and $^2\Phi'_4$ in eqs 6 and 7), indeed, supply a fractional negative spin density on NO, this effect is partially compensated by the other configurations (like $^2\Phi'_2$, $^2\Phi'_5$, and $^2\Phi'_6$ in eqs 6 and 7), which produce a fractional positive spin density on NO. The net effect is a negligible spin density on NO for complexes **1** and **4** and a positive spin density on NO for complex **3** (due to a large contribution of $^2\Phi'_5$ in this case). Also one should not forget that "antiferromagnetic character" (in the sense of the multiconfigurational expansion) and "spin polarization" (in the sense of the spin density) are two different quantities, which although related to each other should not be confused. A spin polarization is always rooted in the presence of antiferromagnetic configurations, but antiferromagnetic configurations do not always generate a spin polarization. The most evident counterexample is an open-shell singlet configuration, which has 100% antiferromagnetic character but produces zero spin density (no polarization).

Let us now compare the CASSCF and DFT spin densities for complexes **1**, **3**, and **4**. For this purpose, Figure 6 shows the Mulliken spin populations in an (x,y)-plot, where the x-axis gives the spin population on NO and the y-axis gives the spin population on Fe. A first look at Figure 6 already reveals that the points for the doublet state concentrate around the $x + y = 1$ line (i.e., the total population of Fe and NO is close to one

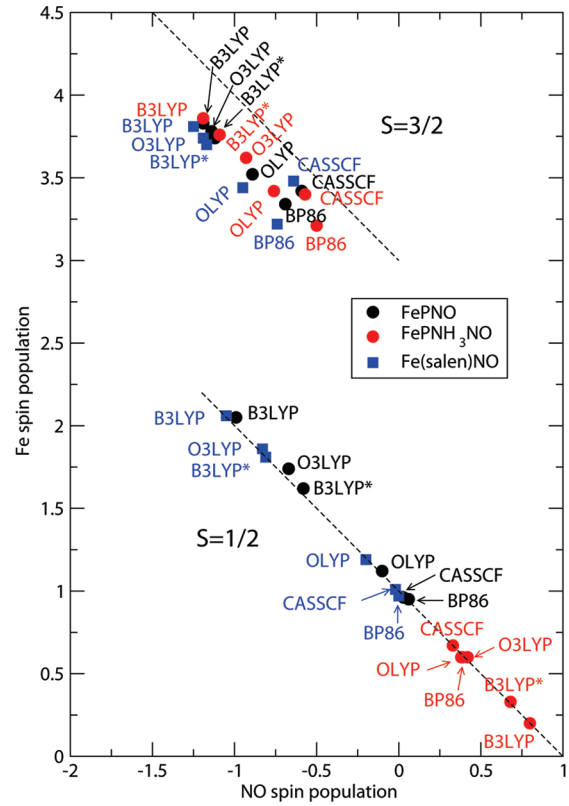

Figure 6. CASSCF and DFT Mulliken spin populations on NO and Fe for FePNO (**1**), $FePNH_3NO$ (**3**), and Fe(salen)NO (**4**).

unpaired electron) and, similarly, the points for the quartet state are close to the $x + y = 3$ line (i.e., three unpaired electrons on Fe and NO in total). However, whereas the $S = 1/2$ points lie very close to their trend line, the $S = 3/2$ points are slightly shifted below, indicating that some spin density is missing from the FeNO group. This can be explained by the single occupation of the d_{xy} orbital in the quartet state (cf. Figure 2 and eq 4 in section 3.1); as this orbital is slightly delocalized onto the equatorial ligands (P, salen, etc.), part of the spin density is located on these ligands rather than on FeNO. N.B., this residual spin density is larger for the DFT calculations than the CASSCF calculations (viz., the DFT points for $S = 3/2$ lie further from the trend line in Figure 6 than for the analogous CASSCF points).[50]

As Figure 6 shows, and in agreement with previous DFT investigations,[2,5,6] the spin populations of the FeNO group are strongly functional dependent. For all three complexes, the nonhybrid functionals predict spin density distributions most closely to CASSCF, and thus probably the most accurate ones. The hybrid functionals point to substantially different spin distributions. With $FePNH_3NO$ (**3**) as an exception, a much stronger spin polarization (majority spin density on Fe and minority spin density on NO) is predicted with hybrid than with nonhybrid functionals. This seems to be a quite general behavior, connected to the fact that admixture of Hartree−Fock exchange in the hybrid functionals favors open shell descriptions with respect to approximate (local) exchange functionals.[22,51,52] Here, the most evident example of this tendency is observed for the spin density distribution in the $S = 1/2$ state of the five-coordinate complexes, which drastically varies when going from the nonhybrid functionals (spin density localized mostly on Fe, no spin polarization) to the hybrid functionals (strong spin polarization).[53]

TABLE 4: Adiabatic Electronic Quartet−Doublet Gaps, ΔE_{el} (in kcal/mol)

	FePNO (**1**)	FePImNO (**2**)	$FePNH_3NO$ (**3**)	Fe(salen)NO (**4**)	Fe(5-Cl-salen)NO (**5**)
BP86	16.7	21.0	20.6	10.2	10.2
OLYP	5.9	8.7	8.9	–0.6	–0.7
O3LYP	–4.0	–0.2	–0.2	–10.1	–10.1
B3LYP*	3.5	9.4	9.4	–3.0	–3.0
B3LYP	–1.2	4.1	4.2	–7.1	–7.1
CASPT2/bs 1	–1.8	1.3	–0.7	–5.7	–5.9
CASPT2/bs 2	1.0	3.1	2.1	–5.2[a]	–5.2[a]
CASPT2/bs 3	3.5	*b*	4.9	–4.9[a]	–5.0[a]
Exptl[c]	≥3.3	≥3.4	≥3.0	2.2	≤1.5

[a] Estimated (see section 2). [b] Calculations too large to be feasible. [c] Using eq 2, either from exptl spin crossover temp. or the lack of spin crossover at room temp. (**1**−**3**) or 0 K (**5**).

Obviously, the "overpolarized" spin densities obtained from hybrid DFT do not agree with the ab initio (CASSCF) spin densities. On the other hand, spin polarization in spin-unrestricted (broken-symmetry) DFT calculations is often taken as a manifestation of antiferromagnetic interactions,[54,55] even though the spin densities themselves are usually unphysical due to limitations of single-determinantal wave function (e.g., a spin-polarized description of singlet-state biradicals, for which the exact spin density must be zero everywhere). Following this interpretation, one may view the spin-polarized description of the FeNO group simply as a way in which the DFT calculations attempt to portray the antiferromagnetic interactions between the Fe and NO fragments. Some antiferromagnetic Fe−NO configurations are indeed also present in the CAS wave function, particularly for the $S = 3/2$ complexes, but also for the $S = 1/2$ complexes (cf. Table 3 in section 3.1). It is interesting that all functionals (hybrid and nonhybrid) predict a noticeable spin polarization for the $S = 3/2$ complexes but that only the hybrid functionals do so for the $S = 1/2$ complexes (**1**, **4**). This fact strongly suggests that the antiferromagnetic character is more pronounced for the $S = 3/2$ than for the $S = 1/2$ complexes, a conclusion in qualitative agreement with the percentage antiferromagnetic character of the CAS wave function (cf. Table 3 in section 3.1). Quite an exceptional behavior is observed for the $S = 1/2$ state of the six-coordinate complex (**3**), for which all functionals point to a spin density *without* any spin polarization. Again, this may be related to the considerably smaller antiferromagnetic character of this system as deduced from the CASSCF wave function (see Table 3). We note, however, that also for this system the actual spin density distribution is strongly functional dependent, being much more localized on NO (80%) for the hybrid functionals than for the nonhybrid ones (only 30%).

3.3. Spin State Energetics. The adiabatic quartet−doublet gap ΔE_{el} for complexes **1**−**5** is given in Table 4. In addition to the DFT and CASPT2 results, this table also contains some experimental results obtained from eq 2 in section 2. For the spin crossover complex Fe(salen)NO (**4**), the experimental ΔE_{el} value was obtained from the spin crossover temperature (T_c = 175 K).[25] For Fe(5-Cl-salen)NO (**5**), no thermal spin crossover is observed.[25] The experimental ΔE_{el} value is therefore an upper bound, knowing that the complex remains in the quartet state even at low temperatures. Similarly, a lower bound on ΔE_{el} for the complexes with heme groups (**1**−**3**) is deduced from the fact that these complexes (**1**−**3**) have an experimental doublet ground state[14,23,48] up to at least room temperature.

Conforming with previous studies,[5,6] the ΔE_{el} results obtained from DFT are strongly functional dependent. In general, nonhybrid functionals predict a much higher quartet−doublet gap (even by ∼20 kcal/mol) than hybrid functionals. In some cases, this leads to a different prediction of the ground state.

Let us first focus on the heme complexes (**1**−**3**). For FePNO (**1**), the expected doublet ground state is correctly predicted by CASPT2, BP86, OLYP, and B3LYP*, while B3LYP and O3LYP point to a quartet ground state. For the six-coordinate complexes (**2**, **3**), all methods except O3LYP yield the correct ground state. Note, however, that ΔE_{el} varies from a few kcal/mol (CASPT2, hybrid functionals) to over 20 kcal/mol (BP86). One can easily note that complexes **2** (with Im) and **3** (with NH_3) are almost identical in terms of quartet−doublet splitting. Obviously, both models of six-coordinate heme−NO complexes are equivalent for the present study. For the five-coordinate complex **1**, the B3LYP* and OLYP results are closest to the CASPT2 result, while for the six-coordinate complexes (**2**, **3**) the agreement seems better for the B3LYP functional. When comparing the DFT and CASPT2 quartet−doublet gaps in Table 4, one must be aware that, whereas the DFT results are already basis set saturated (see section 2), this is not necessarily the case for the CASPT2 results. Wherever available, we refer to the results obtained with the most extensive basis 3, but when extrapolated to complete basis set, the gaps could be higher by a few kcal/mol. This will stabilize the correct (doublet) ground state even more.

It might be interesting to inspect the effect of the axial N donor ligand on ΔE_{el}, i.e., to compare the results for complex **2** (or **3**) with those for complex **1**. Such differential energies may be expected to be less basis set and functional dependent. At the DFT level, the axial ligand effect ranges from 3 to 5 kcal/mol, while at the CASPT2 level it is smaller, only 1−2 kcal/mol. Such a small effect of the axial ligand on the quartet−doublet gap may be somewhat striking, considering its profound influence on the spin densities (see section 3.2). Moreover, in a previous CASPT2 study,[2] we also observed a more considerable effect of the axial ligand on the spin state energetics of the basic heme complexes (FeP, FePIm) as well as on their NO binding energy. The limited size of the effect for this particular case may be brought back to the fact that both in the five- and six-coordinate complexes the doublet-to-quartet transition merely involves an electron transfer within the equatorial plane, from $d_{x^2-y^2}$ to d_{xy} (see section 3.1); therefore, its energy should not be strongly influenced by the presence of an axial ligand.

Let us note here that in a previous B3LYP study[56] the quartet state of the six-coordinate FePImNO heme model was claimed to have a much higher energy (10 kcal/mol above the doublet state) and also a much longer Fe−NO distance (2.9 Å) than found from our B3LYP calculations (4 kcal/mol and 1.8 Å, respectively). This is a serious physical difference in the character of the quartet state, strongly versus weakly bonded, with possible implications on the heme−NO dissociation kinetics.[5,24] We believe that the difference should be attributed to a different DFT formalism: unrestricted (U) in this work,

restricted open-shell (RO) in ref 56. As was shown in section 3.1, bonding of NO in the quartet state is accompanied by strong antiferromagnetic coupling. This must give rise to strong differences in the Fe−NO bond description with both formalisms, given that RODFT cannot capture the antiferromagnetic coupling at all, whereas with UDFT it is manifested by a strong polarization of the spin density (cf. Figure 6). Thus, we think that using an unrestricted approach is more appropriate to describe the quartet spin state.

In contrast to the heme nitrosyls, the Fe(salen)NO complex (**4**) has a doublet ground state only at low temperatures, undergoing a spin crossover to the quartet state at $T_c = 175$ K.[25] The Fe(5-Cl-salen)NO complex (**5**) appears to have a quartet ground state for the whole range of temperatures, with no evidence of thermal spin crossover. First of all, it is surprising that these two complexes have two such different experimental estimates of ΔE_{el}. All of our calculations would rather point to a very similar ΔE_{el} (only 0.0−0.2 kcal/mol difference). Chemical intuition also tells us that the Cl atoms in **5** lie too far to significantly affect the crystal field of the iron ion. We therefore suspect that the difference in the quartet−doublet gap between complexes **4** and **5** is primarily of intermolecular origin. It is possible that both complexes have significantly different intermolecular interactions in their crystal phases. Indeed, complex **5** has a larger molecular volume than **4** (due to the presence of the large Cl atoms) and thus might have a different packing. Unfortunately, since the crystal structure of **5** has not been resolved, we cannot verify this hypothesis.

Comparison of the experimental ΔE_{el} value for Fe(salen)NO with the theoretical gaps indicates that it is extremely difficult to accurately reproduce the experimental value for this complex. The best agreement is achieved for the OLYP functional (−3 kcal/mol error), slightly worse for B3LYP* (−5 kcal/mol error), while other functionals lead to even larger errors: −9 to −12 kcal/mol for B3LYP and O3LYP, and +8 kcal/mol for BP86 (also for PBE,[57] and possibly also for other classical nonhybrid functionals). The CASPT2 result (for basis 3) falls close to B3LYP* and has a rather significant error of −7.1 kcal/mol. The absolute value of the error tends to decrease with increasing basis set. However, somewhat surprising, the basis set dependence is much weaker in this case than for the complexes **1**−**3**. Therefore, we doubt that basis set incompleteness is the most important source of the present error for complex **4**. We further note that errors of ∼5 kcal/mol in favor of the high spin state were already found in previous CASPT2 calculations for transitions which (like the present one) involve an electron transfer from the nonbonding $d_{x^2-y^2}$ to the antibonding d_{xy} orbital, e.g., the $^5A_{1g} \rightarrow {}^3A_{2g}, {}^1A_{1g}$ transitions in FeP[2,18] and the singlet → quintet transition in a series of complexes with $Fe(II)N_6$ architecture.[58] Moreover, our very recent test calculation on small ferrous heme models[8] indicates that, as compared to CCSD(T), CASPT2 also there overstabilizes the quintet with respect to the singlet state by about 5 kcal/mol.[8,59] The problem may be related to the form of the zeroth-order Hamiltonian in CASPT2, although the original bias of CASPT2 in favor of open-shell electronic structures[41] was already practically remedied by shifting the diagonal Fock matrix elements in the present (IPEA) implementation.[60] Finally, it is also possible that the experimental gap estimated for the crystal Fe(salen)NO is not the same as it would be for the free molecule in vacuo (i.e., as we calculated it) due to the intermolecular interactions present in the crystal. In the crystal structure of Fe(salen)NO, the molecules are rather densely packed, the benzene ring of the salen ligand approaching the Fe atom of the neighboring molecule from the bottom.[37] A rigorous treatment of the interactions and their effect on the quartet−doublet gap would be a very demanding project, certainly beyond the scope of the present paper. As already mentioned, the intermolecular interactions supposedly change the difference of ΔE_{el} values for complexes **5** and **4** by about 0.5 kcal/mol. However, this value is only the *relative* effect of the intermolecular interactions on ΔE_{el} of two similar complexes, while the ΔE_{el} values in the individual species may be affected much more (possibly by a few kcal/mol). Let us recall here a large effect of the intermolecular (π-stacking) interactions found in our previous study of the bis(acetylacetonate) cobalt(II) complex.[61]

4. Conclusions

In the present study, we applied CASSCF/CASPT2 and selected DFT methods to some heme and nonheme complexes with the $\{FeNO\}^7$ group in their lowest doublet ($S = 1/2$) and quartet ($S = 3/2$) electronic states. We have taken a look at the character of the wave function at the CASSCF level, interpreted the CASSCF and DFT spin densities, and compared the relative energies of the two spin states.

The analysis of the CASSCF wave function provides insight into the nature of the Fe−NO bond at the multiconfigurational level. The bonding is characterized by strong nondynamic (left−right) correlation and antiferromagnetic interactions between the Fe and NO fragments. Using the localized orbitals of the Fe and NO fragments, the CAS wave function may be decomposed into several resonance structures, among which $Fe(II)-NO^0$ and $Fe(III)-NO^-$ constitute the majority. These two structures have a comparable contribution for all complexes studied, except for the ($S = 3/2$) "brown ring" complex (**7**), which appears to be predominantly $Fe(II)-NO^0$.

The CASSCF spin densities of the heme complexes are in good agreement with available MCD and EPR data;[14,23,48] therefore, they may serve as a reference to assess the quality of the DFT spin densities, which are strongly functional dependent. The closest agreement with CASSCF is found for the nonhybrid functionals. The ab initio spin densities are (in some cases) very sensitive to changes in ligand field and/or the spin state. Nevertheless, we have found no evidence that the observed shifts of spin density between Fe and NO are in any way correlated to net flows of electronic charge, which might lead to a change of oxidation state. On the contrary, the contributions of the dominant $Fe(II)-NO^0$ and $Fe(III)-NO^-$ resonance structures appear to be insensitive to any change of the ligand field and they are pretty much the same for the doublet and the quartet spin states, despite their very different spin densities. This can be treated as a warning not to overinterpret spin densities as a measure of the oxidation state (note an analogous conclusion elsewhere[62]).

The final point of this study was to calculate the quartet−doublet relative energy. Previous studies already indicated that the DFT spin state energetics is extremely sensitive to the choice of the exchange functional, with some indication that OLYP and B3LYP* yield the most accurate results.[5,6,63] This is also confirmed here. The CASPT2 calculations correctly predict the doublet ground state for the heme−NO complexes, with the quartet state about 4−5 kcal/mol higher in energy. However, for Fe(salen)NO, this approach overstabilizes the quartet state by about 7 kcal/mol. The error might be a combination of the method's and basis set error with the influence of the intermolecular interactions on the experimental value. Nevertheless, the error must be put into proper perspective, which is given by even larger errors of the DFT calculations (except for OLYP

and B3LYP* functionals). We note that, even accounting for the suspected error of the CASPT2 calculations, the quartet−doublet gap in the heme−NO complexes (**1**−**3**) is predicted to be at most 11−12 kcal/mol. This is still much smaller than 16−21 kcal/mol predicted by the "classical" nonhybrid functionals. It also means that the excited quartet state of the heme−NO complexes is rather easily accessible, with possible implications on the dynamics of NO binding/dissociation.[5,24]

We hope that the present computational study has shown that CASSCF/CASPT2 calculations are not only feasible for relatively large transition metal complexes of biological importance but also can be useful in the interpretation of their electronic structure. Certainly, the {FeNO}^{7} complexes are electronically very complicated systems, in some sense even "pathological", which highlights the importance of choosing the proper computational methodology. Nevertheless, the problematic aspects of the electronic structure of these complexes (noninnocent ligands, densely lying electronic states, left−right correlation in metal−ligand bond, and antiferromagnetic interactions) are rather common in the bioinorganic area and cannot be escaped from. Therefore, even though DFT will probably remain a "golden standard" of bioinorganic chemistry for a long time (in particular for studying reaction mechanisms), ab initio calculations on moderate sized model complexes also have a promising future in this field.

Acknowledgment. This research project has been supported by the grants from the Flemish Science Foundation (FWO) and from the Concerted Research Action of the Flemish Government (GOA) and by the Polish State Ministry of Science and Higher Education (MNiSW) from the funds for scientific research (2009−2010). The computational grants from the Academic Computer Center CYFRONET AGH are also acknowledged. The molecular graphics in Figure 1 were prepared with the XYZViewer program obtained by courtesy of Sven de Marothy (Stockholm University).

Supporting Information Available: Molecular structures, contour plots of the natural and localized CASSCF orbitals, and Mulliken spin populations. This material is available free of charge via the Internet at http://pubs.acs.org.

References and Notes

(1) Blomberg, L. M.; Blomberg, M. R.; Siegbahn, P. E. *J. Inorg. Biochem.* **2005**, *99*, 949–958.
(2) Radoń, M.; Pierloot, K. *J. Phys. Chem. A* **2008**, *112*, 11824–11832.
(3) Westcott, B. L.; Enemark, J. L. Transition Metal Nitrosyls. In *Inorganic Electronic Structure and Spectroscopy*; Solomon, E. I., Lever, A. B. P., Eds.; Wiley: New York, 1999; Vol. 2.
(4) Ghosh, A. *Acc. Chem. Res.* **2005**, *38*, 943–953.
(5) Ghosh, A. *J. Biol. Inorg. Chem.* **2006**, *11*, 712–724.
(6) Conradie, J.; Ghosh, A. *J. Phys. Chem. B* **2007**, *111*, 12621–12624.
(7) Cheng, H.-Y.; Chang, S.; Tsai, P.-Y. *J. Phys. Chem. A* **2004**, *108*, 358–361.
(8) Olah, J.; Harvey, J. *J. Phys. Chem. A* **2009**, *113*, 7338–7345.
(9) Griffith, W. P.; Lewis, J.; Wilkinson, G. *J. Chem. Soc.* **1958**, *1958*, 3993–3998.
(10) Burlamacchi, L.; Martini, G.; Tiezzi, E. *Inorg. Chem.* **1969**, *8*, 2021–2025.
(11) Ray, M.; Golombek, A. P.; Hendrich, M. P.; Yap, G. P. A.; Liable-Sands, L. M.; Rheingold, A. L.; Borovik, A. S. *Inorg. Chem.* **1999**, *38*, 3110–3115.
(12) Rodriguez, J. H.; Xia, Y.-M.; Debrunner, P. G. *J. Am. Chem. Soc.* **1999**, *121*, 7846–7863.
(13) Wanat, A.; Schneppensieper, T.; Stochel, G.; van Eldik, R.; Bill, E.; Wieghardt, K. *Inorg. Chem.* **2002**, *41*, 4–10.
(14) Praneeth, V.; Neese, F.; Lehnert, N. *Inorg. Chem.* **2005**, *44*, 2570–2572.
(15) Silaghi-Dumitrescu, R.; Silaghi-Dumitrescu, I. *J. Inorg. Biochem.* **2006**, *100*, 161–166.
(16) Roos, B. O.; Taylor, P. R.; Siegbahn, P. E. M. *Chem. Phys.* **1980**, *48*, 157–173.
(17) Andersson, K.; Malmqvist, P.-Å.; Roos, B. O. *J. Chem. Phys.* **1991**, *96*, 1218–1226.
(18) Pierloot, K. *Mol. Phys.* **2003**, *101*, 2083–2094.
(19) Pierloot, K.; Vancoillie, S. *J. Chem. Phys.* **2006**, *125*, 124303.
(20) Pierloot, K.; Vancoillie, S. *J. Chem. Phys.* **2008**, *128*, 034104.
(21) Roos, B. O.; Veryazov, V.; Conradie, J.; Taylor, P. R.; Ghosh, A. *J. Phys. Chem. B* **2008**, *112*, 14099–14102.
(22) Radoń, M.; Broclawik, E. *J. Chem. Theory Comput.* **2007**, *3*, 728–734.
(23) Praneeth, V.; Nather, C.; Peters, G.; Lehnert, N. *Inorg. Chem.* **2006**, *45*, 2795–2811.
(24) Franzen, S. *Proc. Natl. Acad. Sci. U.S.A.* **2002**, *99*, 16754–16759.
(25) Wells, F. V.; McCann, S. W.; Wickman, H. H.; Kessel, S. L.; Hendrickson, D. N.; Feltham, R. D. *Inorg. Chem.* **1982**, *21*, 2306–2311.
(26) Ahlrichs, R.; Horn, H.; Schaefer, A.; Treutler, O.; Haeser, M.; Baer, M.; Boecker, S.; Deglmann, P.; Furche, F. *Turbomole v5.9*; Quantum Chemistry Group, Universitaet Karlsruhe, Germany, 2006.
(27) Frisch, M. J.; Trucks, G. W.; Schlegel, H. B.; Scuseria, G. E.; Robb, M. A.; Cheeseman, J. R.; Montgomery, J. A., Jr.; Vreven, T.; Kudin, K. N.; Burant, J. C.; Millam, J. M.; Iyengar, S. S.; Tomasi, J.; Barone, V.; Mennucci, B.; Cossi, M.; Scalmani, G.; Rega, N.; Petersson, G. A.; Nakatsuji, H.; Hada, M.; Ehara, M.; Toyota, K.; Fukuda, R.; Hasegawa, J.; Ishida, M.; Nakajima, T.; Honda, Y.; Kitao, O.; Nakai, H.; Klene, M.; Li, X.; Knox, J. E.; Hratchian, H. P.; Cross, J. B.; Bakken, V.; Adamo, C.; Jaramillo, J.; Gomperts, R.; Stratmann, R. E.; Yazyev, O.; Austin, A. J.; Cammi, R.; Pomelli, C.; Ochterski, J. W.; Ayala, P. Y.; Morokuma, K.; Voth, G. A.; Salvador, P.; Dannenberg, J. J.; Zakrzewski, V. G.; Dapprich, S.; Daniels, A. D.; Strain, M. C.; Farkas, O.; Malick, D. K.; Rabuck, A. D.; Raghavachari, K.; Foresman, J. B.; Ortiz, J. V.; Cui, Q.; Baboul, A. G.; Clifford, S.; Cioslowski, J.; Stefanov, B. B.; Liu, G.; Liashenko, A.; Piskorz, P.; Komaromi, I.; Martin, R. L.; Fox, D. J.; Keith, T.; Al-Laham, M. A.; Peng, C. Y.; Nanayakkara, A.; Challacombe, M.; Gill, P. M. W.; Johnson, B.; Chen, W.; Wong, M. W.; Gonzalez, C.; Pople, J. A. *Gaussian 03*, revision C.02; Gaussian, Inc.: Wallingford, CT, 2004.
(28) Weigend, F.; Ahlrichs, R. *Phys. Chem. Chem. Phys.* **2005**, *7*, 3297–3305.
(29) Güell, M.; Luis, J. M.; Solà, M.; Swart, M. *J. Phys. Chem. A* **2008**, *112*, 6384–6391.
(30) Becke, A. D. *J. Chem. Phys.* **1993**, *98*, 5648–5652.
(31) Reiher, M.; Salomon, O.; Hess, B. A. *Theor. Chem. Acc.* **2001**, *107*, 48–55.
(32) Cohen, A. J.; Handy, N. C. *Mol. Phys.* **2001**, *99*, 607–615.
(33) Handy, N. C.; Cohen, A. J. *Mol. Phys.* **2001**, *99*, 403–412.
(34) Lee, C.; Yang, W.; Parr, R. G. *Phys. Rev. B* **1988**, *37*, 785–789.
(35) Becke, A. D. *Phys. Rev. A* **1988**, *38*, 3098–3100.
(36) Perdew, J. P. *Phys. Rev. B* **1986**, *33*, 8822–8824.
(37) Haller, K. J.; Johnson, P. L.; Feltham, R. D.; Enemark, J. H.; Ferraro, J. R.; Basile, L. J. *Inorg. Chim. Acta* **1979**, *33*, 119–130.
(38) Andersson, K.; Aquilante, F.; Barysz, M.; Bednarz, E.; Bernhardsson, A.; Blomberg, M. R. A.; Carissan, Y.; Cooper, D. L.; Cossi, M.; Devarajan, A.; De Vico, L.; Ferré, N.; Fülscher, M. P.; Gaenko, A.; Gagliardi, L.; Ghigo, G.; de Graaf, C.; Hess, B. A.; Hagberg, D.; Holt, A.; Karlström, G.; Krogh, J. W.; Lindh, R.; Malmqvist, P.-Å.; Nakajima, T.; Neogrády, P.; Olsen, J.; Pedersen, T. B.; Raab, J.; Reiher, M.; Roos, B. O.; Ryde, U.; Schimmelpfennig, B.; Schütz, M.; Seijo, L.; Serrano-Andrés, L.; Siegbahn, P. E. M.; Stålring, J.; Thorsteinsson, T.; Veryazov, V.; Widmark, P.-O.; Wolf, A. *MOLCAS*, version 7.2, Lund University: Lund, Sweden, 2008.
(39) Roos, B. O.; Lindh, R.; Malmqvist, P.-Å.; Veryazov, V.; Widmark, P.-O. *J. Phys. Chem. A* **2005**, *109*, 6575–6579.
(40) Pierloot, K.; Dumez, B.; Widmark, P.-O.; Roos, B. *Theor. Chim. Acta* **1995**, *90*, 87–114.
(41) Roos, B. O.; Andersson, K.; Fulscher, M.; Malmqvist, P.-Å.; Serrano-Andrés, L.; Pierloot, K.; Merchan, M. *Adv. Chem. Phys.* **1996**, *93*, 219–331.
(42) Aquilante, F.; Pedersen, T. B.; de Meras, A. S.; Koch, H. *J. Chem. Phys.* **2006**, *125*, 174101.
(43) Tuchagues, J.-P.; Bousseksou, A.; Molnár, G.; McGarvey, J. J.; Varret, F. *Top. Curr. Chem.* **2004**, *235*, 85–103.
(44) Paulsen, H.; Trautwein, A. X. *Top. Curr. Chem.* **2004**, *235*, 197–219.
(45) In eqs 5a−5c, the ↑/↓ superscripts denote a spin coupling which, going from left to right, increases/decreases the total spin of the configuration state function by $\Delta S = 1/2$.
(46) Ray, M.; Golombek, A. P.; Hendrich, M. P.; Young, V. G.; Borovik, A. S. *J. Am. Chem. Soc.* **1996**, *118*, 6084–6085.
(47) Tangen, E.; Svadberg, A.; Ghosh, A. *Inorg. Chem.* **2005**, *44*, 7802–7805.
(48) Hayes, R. G.; Ellison, M. K.; Scheidt, W. R. *Inorg. Chem.* **2000**, *39*, 3665–3668.
(49) McGarvey, B. R. *Can. J. Chem.* **1975**, *53*, 2498–2511.

(50) It might be useful to include the residual spin population on the equatorial ligand atoms in the spin population of iron. Such modified spin populations of Fe were also calculated (see the Supporting Information). They lead to very similar conclusions as the original spin populations.

(51) Laming, G. J.; Handy, N. C.; Amos, R. D. *Mol. Phys.* **1993**, *80*, 1121–1134.

(52) Remenyi, C.; Kaupp, M. *J. Am. Chem. Soc.* **2005**, *127*, 11399–11413.

(53) In some previous studies (refs 2 and 64), a non-polarized spin density was reported for the B3LYP calculations on $S = 1/2$ complex **1** (with about 50% of the spin population on NO and the other 50% on Fe). This probably corresponds to a different electromer than the one described in this study, of slightly higher energy (2.3 kcal/mol) and with a slightly shorter (0.1 Å) Fe−NO distance. The values given in parentheses were obtained from B3LYP/B optimizations of both electromers.

(54) Rovira, C.; Kunc, K.; Hutter, J.; Ballone, P.; Parrinello, M. *J. Phys. Chem. A* **1997**, *101*, 8914–8925.

(55) Neese, F. *J. Phys. Chem. Solids.* **2004**, *65*, 781–785.

(56) Strickland, N.; Harvey, J. N. *J. Phys. Chem. B* **2007**, *111*, 841–852.

(57) Perdew, J. P.; Burke, K.; Ernzerhof, M. *Phys. Rev. Lett.* **1996**, *77*, 3865–3868.

(58) Kepenekian, M.; Robert, V.; Guennic, B. L. *J. Chem. Phys.* **2009**, *131*, 114702.

(59) Vancoillie, S.; Zhao, H.; Radoń, M.; Pierloot, K. Performance of CASPT2 and DFT for Relative Spin-State Energetics of Heme Models. *J. Chem. Theory Comput.*, in press.

(60) Ghigo, G.; Roos, B.; Malmqvist, P.-Å. *Chem. Phys. Lett.* **2004**, *396*, 142–149.

(61) Radoń, M.; Srebro, M.; Broclawik, E. *J. Chem. Theory Comput.* **2009**, *5*, 1237–1244.

(62) Popescu, D.-L.; Chanda, A.; Stadler, M.; de Oliveira, F. T.; Ryabov, A. D.; Münck, E.; Bominaar, E. L.; Collins, T. J. *Coord. Chem. Rev.* **2008**, *252*, 2050–2071.

(63) Harvey, J. N. *Annu. Rep. Prog. Chem., Sect. C: Phys. Chem.* **2006**, *102*, 203–226.

(64) Praneeth, V.; Haupt, E.; Lehnert, N. *J. Inorg. Biochem.* **2005**, *99*, 940–948.

JP910220R